JACS
JOURNAL OF THE AMERICAN CHEMICAL SOCIETY

Communication

pubs.acs.org/JACS

$CsPb_{0.9}Sn_{0.1}IBr_2$ Based All-Inorganic Perovskite Solar Cells with Exceptional Efficiency and Stability

Jia Liang,[†] Peiyang Zhao,[†] Caixing Wang,[†] Yanrong Wang,[†] Yi Hu,[†] Guoyin Zhu,[†] Lianbo Ma,[†] Jie Liu,[†,‡] and Zhong Jin*[,†]

[†]Key Laboratory of Mesoscopic Chemistry of MOE, School of Chemistry and Chemical Engineering, Nanjing University, Nanjing, Jiangsu 210023, China

[‡]Department of Chemistry, Duke University, Durham, North Carolina 27708, United States

Supporting Information

ABSTRACT: The emergence of perovskite solar cells (PSCs) has generated enormous interest in the photovoltaic research community. Recently, cesium metal halides ($CsMX_3$, M = Pb or Sn; X = I, Br, Cl or mixed halides) as a class of inorganic perovskites showed great promise for PSCs and other optoelectronic devices. However, $CsMX_3$-based PSCs usually exhibit lower power conversion efficiencies (PCEs) than organic–inorganic hybrid PSCs, due to the unfavorable band gaps. Herein, a novel mixed-Pb/Sn mixed-halide inorganic perovskite, $CsPb_{0.9}Sn_{0.1}IBr_2$, with a suitable band gap of 1.79 eV and an appropriate level of valence band maximum, was prepared in ambient atmosphere without a glovebox. After thoroughly eliminating labile organic components and noble metals, the all-inorganic PSCs based on $CsPb_{0.9}Sn_{0.1}IBr_2$ and carbon counter electrodes exhibit a high open-circuit voltage of 1.26 V and a remarkable PCE up to 11.33%, which is record-breaking among the existing $CsMX_3$-based PSCs. Moreover, the all-inorganic PSCs show good long-term stability and improved endurance against heat and moisture. This study indicates a feasible way to design inorganic halide perovskites through energy-band engineering for the construction of high-performance all-inorganic PSCs.

Organic–inorganic hybrid halide perovskite solar cells (PSCs) have been considered as a promising photovoltaic system for solar energy harvesting. The power conversion efficiency (PCE) record of PSCs has rapidly increased from 3.8% to 22.1%.[1−5] The extensively studied hybrid perovskites usually contain organic cations (e.g., methylammonium (MA^+) and formamidinium (FA^+)) filled in the lead halide frameworks, exhibiting appropriate band gap and strong light absorption.[1−5] However, the large-scale deployment of PSCs is still impractical, due to the poor stability of hybrid perovskites and organic chemicals in hole-transport materials (HTMs) under environmental stresses, such as moisture, oxygen, heat, and ultraviolet (UV) light.[5−7]

One viable way to improve the stability of metal halide perovskites (with the general formula ABX_3) is to replace the organic cations (e.g., MA^+ and FA^+) at A sites with inorganic cations, such as cesium (Cs^+) and rubidium (Rb^+) ions. For instances, many mixed-cation perovskites (e.g., Cs/MA-, Cs/FA-, Cs/MA/FA-, and Cs/Rb/MA/FA-based metal halides) were put forward and exhibited good properties.[8−12] However, these mixed-cation perovskites still contain organic cations; hence, the stability of corresponding PSCs are usually not satisfactory, especially under high temperature. The ultimate solution is to completely replace the organic cations with inorganic cations. Recently, inorganic halide perovskites with the formula $CsMX_3$ are drawing great attention for employing in PSCs.[13−30] The properties and stability of $CsMX_3$ are also varied. For example, $CsPbBr_3$ exhibits good stability but with a large band gap (~2.3 eV),[14−17] while $CsPbI_3$ and $CsPbI_2Br$ display relatively narrow band gaps (~1.73 and 1.92 eV),[18−25] but the stability is poor. So far, the PCEs of $CsMX_3$ based PSCs are still inferior to organic–inorganic hybrid PSCs. It is very desirable to rationally design novel inorganic halide perovskites with more favorable energy band levels and stability.

Herein, we report the synthesis of a novel Cs-based inorganic perovskite, $CsPb_{0.9}Sn_{0.1}IBr_2$, through a convenient two-step sequential solution-phase process in ambient air without the need for a glovebox or humidity control. This new mixed-Pb/Sn mixed-halide perovskite has a suitable band gap (1.79 eV) close to that of $CsPbI_3$, but with superior stability. Furthermore, both labile organic HTMs and expensive noble metal electrodes were replaced by highly stable and conductive carbon electrodes. As a result, the all-inorganic PSCs with layered configurations of fluorine doped tin oxide (FTO)/compact TiO_2 (c-TiO_2)/mesoporous TiO_2 (m-TiO_2)/$CsPb_{0.9}Sn_{0.1}IBr_2$/carbon exhibit a large open-circuit voltage (V_{OC}) of 1.26 V and a remarkable PCE of 11.33%, and show good stability against heat (as high as 100 °C) and humidity.

Figure 1a shows the crystal structure of Cs-based inorganic perovskites with the general formula $CsMX_3$, in which the A sites are occupied by Cs^+ ions, B sites are occupied by divalent metal ions (Pb^{2+} or Sn^{2+}), and X sites are occupied by halide ions. The valence band maximum (VBM) of $CsMX_3$ is mainly composed of antibonding hybridization B 6s and X *n*p orbitals with dominant contributions from X *n*p, while the conduction band minimum (CBM) is determined by antibonding mixing of B 6p and X *n*p orbitals, with a major contribution from B 6p.[31] In contrast, the cations at A sites have negligible effect on VBM or CBM. For turning the band structure of $CsMX_3$, we started from $CsPbBr_3$

Received: July 28, 2017
Published: September 21, 2017

DOI: 10.1021/jacs.7b07949
J. Am. Chem. Soc. 2017, 139, 14009−14012

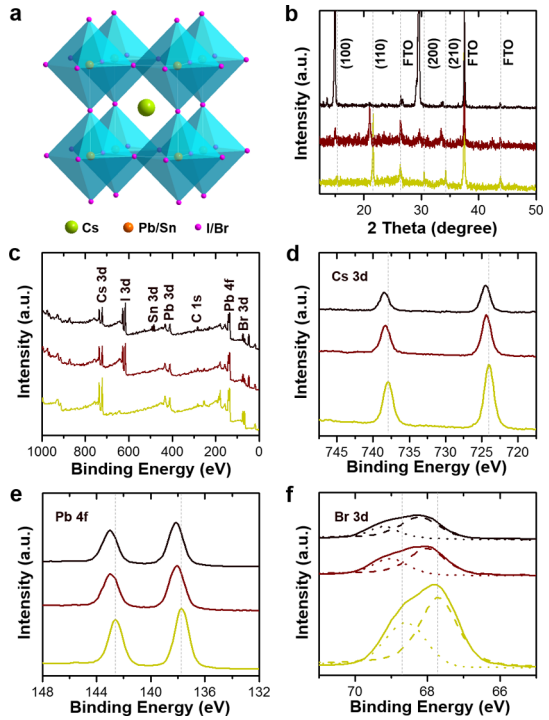

Figure 1. (a) Crystal structure of Cs-based mixed-Pb/Sn mixed-I/Br inorganic perovskites. (b) XRD patterns and (c) survey XPS spectra of $CsPbBr_3$ (yellow lines), $CsPbIBr_2$ (burgundy lines), and $CsPb_{0.9}Sn_{0.1}IBr_2$ (black lines) films, respectively. The peaks marked with "FTO" in (b) are derived from FTO. (d–e) High-resolution XPS spectra of the samples at (d) Cs 3d, (e) Pb 4f, and (f) Br 3d regions, respectively.

because of its superior stability. First, 1/3 of Br^- ions were substituted with I^- ions to shift the VBM toward a more positive level. Second, Pb^{2+} ions were partially substituted by Sn^{2+} ions to shift the CBM toward a more negative level. By adjusting the compositions of the precursor mixture, the appropriate ratio of Pb/Sn was determined to be 0.9:0.1; thus, a mixed-Pb/Sn mixed-I/Br perovskite with the formula of $CsPb_{0.9}Sn_{0.1}IBr_2$ was synthesized. Meanwhile, $CsPbBr_3$ and $CsPbIBr_2$ films were prepared as two control samples.

The crystal structures of inorganic perovskite films were characterized by X-ray diffraction (XRD) (Figure 1b). For $CsPbBr_3$, the XRD peaks were indexed to cubic perovskite-phase $CsPbBr_3$. The XRD peaks of $CsPbIBr_2$ and $CsPb_{0.9}Sn_{0.1}IBr_2$ shifted to small angles, due to the expansion of unit cells induced by I^- ions. For $CsPb_{0.9}Sn_{0.1}IBr_2$, the intensities of (100) and (200) peaks were highly increased, indicating the crystal domains were highly oriented along the (100) planes. Scanning electron microscopy (SEM) images of the films show continuous surface without obvious pinholes (Figure S1).

X-ray photoelectron spectroscopy (XPS) analysis was also performed (Figure 1c–f). The XPS spectrum of $CsPbIBr_2$ showed I 3d peak, and the XPS spectrum of $CsPb_{0.9}Sn_{0.1}IBr_2$ presented I 3d and Sn 3d peaks, indicating the successful introduction of I^- and Sn^{2+} ions, in line with energy dispersive X-ray spectroscopy (EDX) analysis (Figure S2). After setting the C 1s peaks of adventitious carbon to 284.6 eV (Figure S3a), the high-resolution XPS spectra at Cs 3d, Pb 4f, Br 3d, I 3d, and Sn 3d regions were compared in Figure 1d–f and Figure S3b,c, respectively. The characteristic binding energies of these elements are listed in Table S1. The Cs 3d, Pb 4f, and Br 3d peaks of $CsPbIBr_2$ and $CsPb_{0.9}Sn_{0.1}IBr_2$ shifted to higher binding energies (Figure 1d–f), due to the introduction of I^- ions and the changes of chemical bonding, which is consistent with the expanded lattice parameters confirmed by XRD. Moreover, the intensities of Br 3d peaks of $CsPbIBr_2$ and $CsPb_{0.9}Sn_{0.1}IBr_2$ decreased greatly (Figure 1f). However, when the Sn^{2+} ions were introduced, no obvious peak shift was observed from $CsPb_{0.9}Sn_{0.1}IBr_2$, owing to the small substitution ratio of Sn^{2+} ions.

The effects of I^- and Sn^{2+} substitution on the photophysical properties were investigated. Figure 2a presented the colors of the

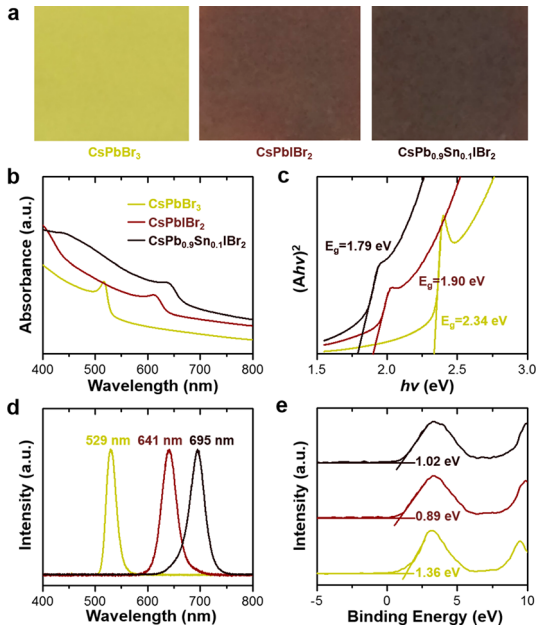

Figure 2. (a) Optical images, (b) UV–Vis absorption spectra, (c) $(Ahv)^2$ vs hv curves, (d) PL spectra, and (e) valence band XPS spectra of $CsPbBr_3$, $CsPbIBr_2$, and $CsPb_{0.9}Sn_{0.1}IBr_2$ films, respectively.

samples, indicating the enhanced visible-light absorption of $CsPbIBr_2$ and $CsPb_{0.9}Sn_{0.1}IBr_2$ films. The UV–Vis absorption spectrum of $CsPbIBr_2$ showed a red shift and improved absorbance after the introduction of I^- ions (Figure 2b). As the Sn^{2+} ions were introduced, a further red shift and higher absorbance were observed, indicating both I^- and Sn^{2+} ions led to a narrower band gap and stronger absorbance. Figure 2c shows the plots of $(Ahv)^2$ vs photon energy (hv) converted from the UV–Vis absorption spectra. The band gaps of $CsPbBr_3$, $CsPbIBr_2$, and $CsPb_{0.9}Sn_{0.1}IBr_2$ were measured to be 2.34, 1.90, and 1.79 eV, respectively. The band gap of $CsPb_{0.9}Sn_{0.1}IBr_2$ is close to that of $CsPbI_3$ (1.73 eV).[18−23] Photoluminescence (PL) spectra of the samples were measured with an excitation wavelength of 450 nm (Figure 2d), showing sharp emission peaks around 529, 641, and 695 nm, respectively, in accordance with the as-measured band gaps. To determine the exact VBM positions, valence band XPS spectra were collected (Figure 2e). Combined with the band gaps obtained from Figure 2b–d, the VBM and CBM positions of the samples were determined, as shown in Figure S4.

The as-obtained inorganic perovskite films were separately used as the light absorbers in all-inorganic PSCs with the functional layers of FTO/c-TiO_2/m-TiO_2/$CsMX_3$/carbon (Figure 3a). All the organic components in conventional hybrid PSCs were eliminated, thus the instability (especially against heat) and expensive cost were reduced. Low-cost carbon electrodes with

DOI: 10.1021/jacs.7b07949
J. Am. Chem. Soc. 2017, 139, 14009–14012

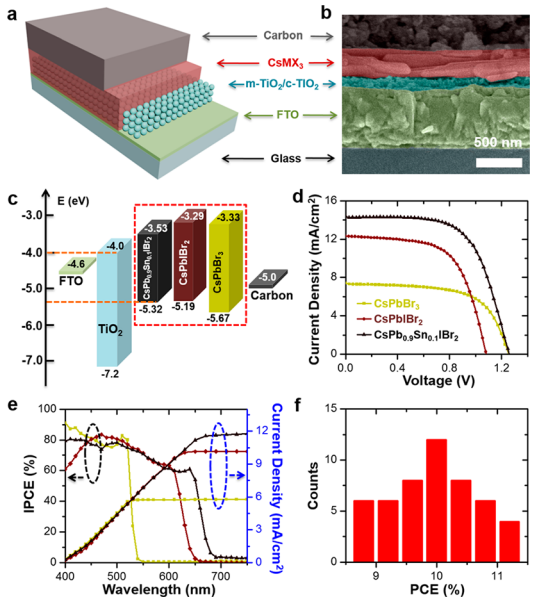

Figure 3. (a) Schematic view and (b) cross-sectional SEM image of all-inorganic PSCs with the configuration of FTO/c-TiO_2/m-TiO_2/$CsMX_3$/carbon. (c) Energy level diagrams of all-inorganic PSCs. The band levels of different $CsMX_3$ perovskites are shown in the red dashed-line box. (d) J–V plots and (e) IPCE spectra and integrated current densities of all-inorganic PSCs based on $CsPbBr_3$, $CsPbIBr_2$, and $CsPb_{0.9}Sn_{0.1}IBr_2$, respectively. (f) Statistical histogram of PCEs obtained from 50 individual $CsPb_{0.9}Sn_{0.1}IBr_2$ based all-inorganic PSCs.

high conductivity, stability, and processability were used to replace both instable organic HTMs and expensive noble metal electrodes for hole collection, since it has a proper work function (−5.0 eV) comparable to gold (−5.1 eV).[16,17] Cross-sectional SEM image of $CsPb_{0.9}Sn_{0.1}IBr_2$ based all-inorganic PSCs depicts the uniform stack of functional layers (Figure 3b). The thickness of $CsPb_{0.9}Sn_{0.1}IBr_2$ film is ∼300 nm. The plane-view SEM images of other functional layers (c-TiO_2, m-TiO_2, and carbon) are shown in Figure S5. Figure 3c shows the energy band levels of all-inorganic PSCs with different light absorbers, exhibiting the electron extraction from the CBM of $CsMX_3$ to that of c-TiO_2/m-TiO_2 electron transfer layers (ETLs) and the hole extraction from the VBM of $CsMX_3$ to that of carbon electrode.

The photocurrent density–voltage (J–V) plots of all-inorganic PSCs with different light absorbers are shown in Figure 3d, and the corresponding photovoltaic parameters are listed in Table S2. The $CsPbBr_3$ based all-inorganic PSCs exhibited a typical PCE of 5.82%, comparable to the previous results (Table S3).[14−17] Owing to the substitution of I^- ions, the $CsPbIBr_2$ based all-inorganic PSCs presented a higher PCE of 8.25%, superior to the reported PSCs based on $CsPbIBr_2$ and organic HTMs.[26,27] When Sn^{2+} ions were further introduced, the $CsPb_{0.9}Sn_{0.1}IBr_2$ based all-inorganic PSCs displayed clear increases in all parameters, including V_{OC} (1.26 V), short-circuit density (J_{SC}, 14.30 mA/cm^2), and fill factor (FF, 0.63). The highest PCE of $CsPb_{0.9}Sn_{0.1}IBr_2$ based all-inorganic PSCs reaches 11.33%, higher than the existing PSCs based on other $CsMX_3$ perovskites (Table S3). Intriguingly, the V_{OC} of $CsPb_{0.9}Sn_{0.1}IBr_2$ based all-inorganic PSCs (1.26 V) is higher than those of $CsPbIBr_2$ (1.08 V) and $CsPbBr_3$ (1.25 V), although the latter have wider band gaps. This is because the V_{OC} is mainly determined by the energy difference between the VBM of the electron donor ($CsMX_3$ in our case) and the CBM of the electron acceptor (TiO_2 in our case). The deep-lying VBM of $CsPb_{0.9}Sn_{0.1}IBr_2$ is ∼0.13 eV lower than that of $CsPbIBr_2$ (Figure 3c); therefore, the $CsPb_{0.9}Sn_{0.1}IBr_2$ based PSCs yield a higher V_{OC} than that of $CsPbIBr_2$, in spite of the narrower band gap. However, although the VBM of $CsPbBr_3$ is the lowest, the V_{OC} of $CsPbBr_3$ based PSCs is comparable to that of $CsPb_{0.9}Sn_{0.1}IBr_2$, possibly owing to the large charge-transfer resistance of $CsPbBr_3$.

Figure 3e shows the incident photo-to-electric current conversion efficiency (IPCE) spectra and integrated current densities of all-inorganic PSCs. Similar to the UV–Vis absorption and PL spectra (Figure 2b, d), the IPCE onset wavelength of $CsPb_{0.9}Sn_{0.1}IBr_2$ exhibits an obvious red shift compared to $CsPbBr_3$ and $CsPbIBr_2$. The integrated J_{SC} values of all-inorganic PSCs based on $CsPbBr_3$, $CsPbIBr_2$, and $CsPb_{0.9}Sn_{0.1}IBr_2$ are calculated to be 5.78, 10.15, and 10.78 mA/cm^2, respectively, which are lower than the J_{SC} values measured from the J–V plots (Figure 3d and Table S2), mainly because the IPCE data in the UV region (wavelength <400 nm) could not be obtained due to the instrument limitation.

The J–V plots of a $CsPb_{0.9}Sn_{0.1}IBr_2$ based all-inorganic PSC were measured by the forward and reverse scan modes (Figure S6a), revealing a minor hysteresis. The J–t and PCE–t curves measured at a fixed voltage of 0.85 V exhibit stable levels (Figure S6b), confirming the good output stability. The J–V histograms of 50 individual $CsPb_{0.9}Sn_{0.1}IBr_2$ based all-inorganic PSCs show a narrow PCE distribution with an average value of 10.0% (Figure S7, Table S4, and Figure 3f), indicating the high repeatability of fabrication.

The long-term stability and heat endurance of $CsPb_{0.9}Sn_{0.1}IBr_2$ based all-inorganic PSCs were evaluated. After sealing with cover glasses and Surlyn spacers, the time-dependent PCE retentions were measured at room temperature (RT) (Figure 4a). The

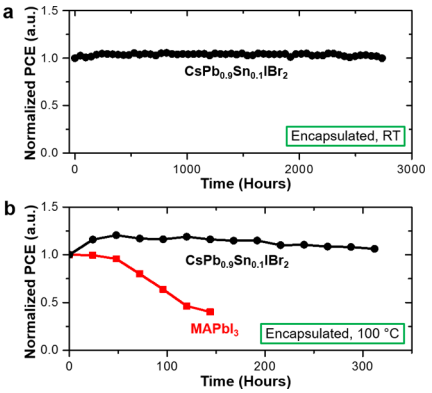

Figure 4. (a) Normalized PCE retentions of encapsulated $CsPb_{0.9}Sn_{0.1}IBr_2$ based all-inorganic PSCs kept at RT. (b) Normalized PCE retentions of encapsulated $CsPb_{0.9}Sn_{0.1}IBr_2$ based all-inorganic PSCs and $MAPbI_3$/carbon based PSCs continuously heated at 100 °C.

encapsulated PSCs exhibited almost no degradation after being kept for >3 months at RT. Moreover, the $CsPb_{0.9}Sn_{0.1}IBr_2$ based all-inorganic PSCs can operate normally even after being continuously heated at 100 °C for >2 weeks (Figure 4b), which cannot be achieved by organic–inorganic hybrid perovskites (such as $MAPbI_3$).[16,17] Intriguingly, the FF show a recognizable increase after heating at 100 °C (Figure S8), which may be ascribed to the improved crystallinity of $CsPb_{0.9}Sn_{0.1}IBr_2$ and the enhanced interfacial interaction between $CsPb_{0.9}Sn_{0.1}IBr_2$ and the carbon electrode by annealing. The stability of $CsPb_{0.9}Sn_{0.1}IBr_2$ based all-inorganic PSCs was also tested without encapsulation

DOI: 10.1021/jacs.7b07949
J. Am. Chem. Soc. 2017, 139, 14009–14012

(Figure S9). After exposure to ambient air with 50−60% relative humidity at RT for 50 h, the PCE retains 85% of its initial value, indicating a moisture resistance superior to $CsPbI_3$ and $CsPbI_2Br$.[18−25]

To evaluate the influence of I/Br contents, $CsPb_{0.9}Sn_{0.1}I_2Br$ films with an I/Br ratio of 2:1 were also prepared; however, these films cannot convert to perovskite phase by thermal annealing (Figure S10), indicating the phase stability of perovskite-phase $CsPb_{0.9}Sn_{0.1}I_2Br$ is inferior to $CsPbBr_3$[16,17] and $CsPb_{0.9}Sn_{0.1}IBr_2$. Moreover, $Cs_{0.9}MA_{0.1}Pb_{0.9}Sn_{0.1}IBr_2$ films doped by MA^+ cations were also prepared but exhibited poor stability (Figure S11), due to the presence of labile MA^+ ions.

In summary, a new mixed-Pb/Sn mixed-I/Br inorganic perovskite, $CsPb_{0.9}Sn_{0.1}IBr_2$, was successfully prepared via a facile solution-phase process. This new perovskite has superb energy band positions and a reasonable band gap, thus beneficial to light absorption and V_{OC}. Moreover, the disadvantages of instable organic components and expensive noble metal electrodes were avoided by adopting carbon electrodes. The $CsPb_{0.9}Sn_{0.1}IBr_2$ based all-inorganic PSCs exhibited an exceptional PCE compared to other $CsMX_3$ based PSCs and demonstrated good long-term stability and resistibility against heat and moisture. The fabrication process is highly reproducible, scalable, convenient, and inexpensive for batch production, without the need for a glovebox or thermal evaporator. We hope this study will promote further research and industrial applications of photovoltaic and optoelectronic devices based on all-inorganic halide perovskites.

■ ASSOCIATED CONTENT

Supporting Information

The Supporting Information is available free of charge on the ACS Publications website at DOI: 10.1021/jacs.7b07949.

Experimental details, additional tables and figures (PDF)

■ AUTHOR INFORMATION

Corresponding Author

*zhongjin@nju.edu.cn

ORCID

Jie Liu: 0000-0003-0451-6111

Zhong Jin: 0000-0001-8860-8579

Notes

The authors declare no competing financial interest.

■ ACKNOWLEDGMENTS

This work is supported by National Key R&D Program of China (2017YFA0208200, 2016YFB0700600, 2015CB659300), Projects of NSFC (21403105, 21573108), Natural Science Foundation of Jiangsu Province (BK20160647), and Fundamental Research Funds for the Central Universities (020514380107).

■ REFERENCES

(1) Kim, H.; Lee, C.; Im, J.; Lee, K.; Moehl, T.; Marchioro, A.; Moon, S.; Humphry-Baker, R.; Yum, J.; Moser, J.; Gratzel, M.; Park, N. *Sci. Rep.* **2012**, *2*, 591.

(2) Burschka, J.; Pellet, N.; Moon, S.-J.; Humphry-Baker, R.; Gao, P.; Nazeeruddin, M. K.; Graetzel, M. *Nature* **2013**, *499*, 316.

(3) Chen, W.; Wu, Y.; Yue, Y.; Liu, J.; Zhang, W.; Yang, X.; Chen, H.; Bi, E.; Ashraful, I.; Graetzel, M.; Han, L. *Science* **2015**, *350*, 944.

(4) Zhang, D.; Yu, Y.; Bekenstein, Y.; Wong, A. B.; Alivisatos, A. P.; Yang, P. *J. Am. Chem. Soc.* **2016**, *138*, 13155.

(5) Song, T.-B.; Yokoyama, T.; Stoumpos, C. C.; Logsdon, J.; Cao, D. H.; Wasielewski, M. R.; Aramaki, S.; Kanatzidis, M. G. *J. Am. Chem. Soc.* **2017**, *139*, 836.

(6) Yang, Y.; You, J. *Nature* **2017**, *544*, 155.

(7) Tsai, H.; Nie, W.; Blancon, J.-C.; Stoumpos, C. C.; Asadpour, R.; Harutyunyan, B.; Neukirch, A. J.; Verduzco, R.; Crochet, J. J.; Tretiak, S.; Pedesseau, L.; Even, J.; Alam, M. A.; Gupta, G.; Lou, J.; Ajayan, P. M.; Bedzyk, M. J.; Kanatzidis, M. G. *Nature* **2016**, *536*, 312.

(8) Choi, H.; Jeong, J.; Kim, H.-B.; Kim, S.; Walker, B.; Kim, G.-H.; Kim, J. Y. *Nano Energy* **2014**, *7*, 80.

(9) Lee, J.-W.; Kim, D.-H.; Kim, H.-S.; Seo, S.-W.; Cho, S. M.; Park, N.-G. *Adv. Energy Mater.* **2015**, *5*, 1501310.

(10) Yi, C.; Luo, J.; Meloni, S.; Boziki, A.; Ashari-Astani, N.; Graetzel, C.; Zakeeruddin, S. M.; Roethlisberger, U.; Graetzel, M. *Energy Environ. Sci.* **2016**, *9*, 656.

(11) Saliba, M.; Matsui, T.; Seo, J.-Y.; Domanski, K.; Correa-Baena, J.-P.; Nazeeruddin, M. K.; Zakeeruddin, S. M.; Tress, W.; Abate, A.; Hagfeldt, A.; Gratzel, M. *Energy Environ. Sci.* **2016**, *9*, 1989.

(12) Saliba, M.; Matsui, T.; Domanski, K.; Seo, J.-Y.; Ummadisingu, A.; Zakeeruddin, S. M.; Correa-Baena, J.-P.; Tress, W. R.; Abate, A.; Hagfeldt, A.; Gratzel, M. *Science* **2016**, *354*, 206.

(13) Liang, J.; Liu, J.; Jin, Z. *Solar RRL* **2017**, 1700086.

(14) Kulbak, M.; Cahen, D.; Hodes, G. *J. Phys. Chem. Lett.* **2015**, *6*, 2452.

(15) Kulbak, M.; Gupta, S.; Kedem, N.; Levine, I.; Bendikov, T.; Hodes, G.; Cahen, D. *J. Phys. Chem. Lett.* **2016**, *7*, 167.

(16) Liang, J.; Wang, C.; Wang, Y.; Xu, Z.; Lu, Z.; Ma, Y.; Zhu, H.; Hu, Y.; Xiao, C.; Yi, X.; Zhu, G.; Lv, H.; Ma, L.; Chen, T.; Tie, Z.; Jin, Z.; Liu, J. *J. Am. Chem. Soc.* **2016**, *138*, 15829.

(17) Liang, J.; Wang, C.; Wang, Y.; Xu, Z.; Lu, Z.; Ma, Y.; Zhu, H.; Hu, Y.; Xiao, C.; Yi, X.; Zhu, G.; Lv, H.; Ma, L.; Chen, T.; Tie, Z.; Jin, Z.; Liu, J. *J. Am. Chem. Soc.* **2017**, *139*, 2852.

(18) Eperon, G. E.; Paterno, G. M.; Sutton, R. J.; Zampetti, A.; Haghighirad, A. A.; Cacialli, F.; Snaith, H. J. *J. Mater. Chem. A* **2015**, *3*, 19688.

(19) Swarnkar, A.; Marshall, A. R.; Sanehira, E. M.; Chernomordik, B. D.; Moore, D. T.; Christians, J. A.; Chakrabarti, T.; Luther, J. M. *Science* **2016**, *354*, 92.

(20) Luo, P.; Xia, W.; Zhou, S.; Sun, L.; Cheng, J.; Xu, C.; Lu, Y. *J. Phys. Chem. Lett.* **2016**, *7*, 3603.

(21) Frolova, L. A.; Anokhin, D. V.; Piryazev, A. A.; Luchkin, S. Y.; Dremova, N. N.; Stevenson, K. J.; Troshin, P. A. *J. Phys. Chem. Lett.* **2017**, *8*, 67.

(22) Kim, Y. G.; Kim, T.-Y.; Oh, J. H.; Choi, K. S.; Kim, Y.-J.; Kim, S. Y. *Phys. Chem. Chem. Phys.* **2017**, *19*, 6257.

(23) Liang, J.; Wang, C.; Zhao, P.; Lu, Z.; Ma, Y.; Xu, Z.; Wang, Y.; Zhu, H.; Hu, Y.; Zhu, G.; Ma, L.; Chen, T.; Tie, Z.; Liu, J.; Jin, Z. *Nanoscale* **2017**, *9*, 11841.

(24) Sutton, R. J.; Eperon, G. E.; Miranda, L.; Parrott, E. S.; Kamino, B. A.; Patel, J. B.; Horantner, M. T.; Johnston, M. B.; Haghighirad, A. A.; Moore, D. T.; Snaith, H. J. *Adv. Energy Mater.* **2016**, *6*, 1502458.

(25) Beal, R. E.; Slotcavage, D. J.; Leijtens, T.; Bowring, A. R.; Belisle, R. A.; Nguyen, W. H.; Burkhard, G. F.; Hoke, E. T.; McGehee, M. D. *J. Phys. Chem. Lett.* **2016**, *7*, 746.

(26) Ma, Q.; Huang, S.; Wen, X.; Green, M. A.; Ho-Baillie, A. W. Y. *Adv. Energy Mater.* **2016**, *6*, 1502202.

(27) Lau, C. F. J.; Deng, X.; Ma, Q.; Zheng, J.; Yun, J. S.; Green, M. A.; Huang, S.; Ho-Baillie, A. W. Y. *ACS Energy Lett.* **2016**, *1*, 573.

(28) Nam, J. K.; Chai, S. U.; Cha, W.; Choi, Y. J.; Kim, W.; Jung, M. S.; Kwon, J.; Kim, D.; Park, J. H. *Nano Lett.* **2017**, *17*, 2028.

(29) Kumar, M. H.; Dharani, S.; Leong, W. L.; Boix, P. P.; Prabhakar, R. R.; Baikie, T.; Shi, C.; Ding, H.; Ramesh, R.; Asta, M.; Graetzel, M.; Mhaisalkar, S. G.; Mathews, N. *Adv. Mater.* **2014**, *26*, 7122.

(30) Song, T.-B.; Yokoyama, T.; Stoumpos, C. C.; Logsdon, J.; Cao, D. H.; Wasielewski, M. R.; Aramaki, S.; Kanatzidis, M. G. *J. Am. Chem. Soc.* **2017**, *139*, 836.

(31) Brandt, R. E.; Stevanovic, V.; Ginley, D. S.; Buonassisi, T. *MRS Commun.* **2015**, *5*, 265.

DOI: 10.1021/jacs.7b07949
J. Am. Chem. Soc. 2017, 139, 14009−14012